Desalination and Water Treatment
www.deswater.com
doi: 10.1080/19443994.2014.918904

55 (2015) 448–462
June

Taylor & Francis
Taylor & Francis Group

Resource utilization of water treatment residual sludge (WTRS): effective defluoridation from aqueous solution

Yumei Zhang[a], Lan Yang[a,c], Dongtian Wang[a,b,*], Tao Zhang[d]

[a]*College of Chemical, Biological and Materials Engineering, Suzhou University of Science and Technology, Suzhou 215009, Jiangsu Province, China, Tel. +86 18862105370; emails: jinshazh_2008@126.com (Y. Zhang), yanglan69@sina.com (L. Yang), dongtianw@163.com (D. Wang)*
[b]*Jiangsu Key Laboratory of Environmental Science and Engineering, College of Environmental Engineering, Suzhou University of Science and Technology, Suzhou 215009, Jiangsu Province, China*
[c]*College of Chemical Engineering and Material, Zhejiang University of Technology, Hangzhou 310014, Zhejiang Province, China*
[d]*Jiangsu Optoelectronic Functional Materials and Engineering Laboratory, College of Chemistry and Chemical Engineering, Southeast University, Nanjing 211189, Jiangsu Province, China, email: zhangtaochem@163.com*

Received 12 December 2013; Accepted 20 April 2014

ABSTRACT

For resource utilization, water treatment residual sludge (WTRS) and its cerium-modified product (Ce-WTRS) were used as adsorbents to remove F^- from aqueous solution. The adsorbent materials were characterized by energy dispersive X-ray, scanning electron microscope, X-ray diffraction, Fourier transform infrared, and specific surface area test techniques. Different experimental conditions such as pH, initial F^- concentration, contract time, and temperature were investigated. The appropriate adsorption capacity was achieved in the pH range of 3–9. Adsorption kinetics, isotherm, and thermodynamic studies were used to illustrate the nature of F^- onto adsorbents materials. Good fitting of pseudo-second-order kinetics model indicated the chemisorption nature. Further analyses of intra-particle diffusion model were carried out to determine the rate controlling step. It was found that the Langmuir and Temkin isotherm models fitted the experimental data better. The maximum adsorption capacity (q_m) determined by Langmuir isotherm model was 15.45 mg/g for Ce-WTRS, 22% higher than WTRS. The negative values of ΔG^θ indicated the feasibility and spontaneity of material-fluoride interaction. $\Delta H^\theta > 0$ for Ce-WTRS demonstrated the endothermic nature, while $\Delta H^\theta < 0$ for WTRS suggested an exothermic procedure. Ion exchange and complex reaction were identified as the main mechanism of fluoride adsorption.

Keywords: Fluoride; Adsorption; Water treatment residual sludge; Cerium modification; Characterization; Kinetics; Isotherm

1. Introduction

Water treatment residual sludge (WTRS) is a waste by-product of the drinking water treatment processes. Typically, the waterworks sludge contains soil particle, colloidal material, microbial species, residues of other chemicals (i.e. polymers), and cationic flocculation. These compositions and groups have made WTRS a potential adsorbent for harmful ions removal. Previous studies have reported the ability

*Corresponding author.

of WTRS to remove harmful ions such as phosphate [1–4], perchlorate [5], and heavy metal [6,7].

Excessive fluoride ions in water bodies pose a great threat to the living environment and health of human beings nowadays. It is estimated that more than 200 million people worldwide rely on drinking water with fluoride concentrations exceeding the WHO guideline of 1.5 mg/L. Long-term ingestion of fluoride-rich drinking water causes serious health disorders such as mottling of teeth, softening of bones, and ossification of tendons and ligaments, and various neurologic damages [8]. To reduce fluoride concentration in naturally high fluoride waters or fluoride contaminated waters, a variety of methods have been developed, including electrocoagulation [9,10], electrodialysis [11], precipitation [12], ion exchange [13], reverse osmosis [14], and Donnan dialysis [15]. Among these methods, electrocoagulation, electrodialysis, and reverse osmosis show excellent capacity for F^- removal, but require very high capital cost. Precipitation is most widely used, but it is inefficient and always causes secondary pollution. Adsorption is generally considered attractive because of its effectiveness, low cost, simple procedure, and sustainable method [16,17].

A recent statement has shown that materials containing rare earth elements are projected as potential adsorbents mainly due to their strong affinity specifically towards fluoride [18]. Zhang et al. [19] have used CeO_2/Al_2O_3 composites as fluoride adsorbents and investigated the adsorption mechanism of fluoride onto CeO_2/Al_2O_3 composites. Swain et al. [20] have utilized Zr(IV)–ethylenediamine to remove fluoride from water. Onyango et al. [21] have employed La^{3+}-exchanged zeolite to remove the excess fluoride in natural groundwater. Swain et al. [22] have studied the adsorption of fluoride in drinking water by using cerium-impregnated chitosan as adsorbent. These rare earth-loaded adsorbents are proved to be rather efficient for fluoride removal.

For resource utilization, WTRS and its Ce(III)-modified product (Ce-WTRS) were used as the adsorbents for fluoride removal. The experimental data were then fitted to kinetic and isotherm models to understand the mechanism of fluoride onto WTRS and Ce-WTRS.

2. Materials and methods

2.1. Main reagents

Sodium fluoride (NaF), sodium hydroxide (NaOH), hydrochloric acid (HCl), and sodium chloride (NaCl) were purchased from Fine Chemical Materials, Shanghai, China. Ethylic acid (HAc), sodium acetate (NaAc), and sodium citrate ($C_6H_5Na_3O_7{\cdot}2H_2O$) were procured from Kermel Chemical Reagent Ltd Tianjin, China. Cerium nitrate hexahydrate [$Ce(NO_3)_3{\cdot}6H_2O$] was purchased from Aladdin reagent, Shanghai, China. Total ionic strength adjustment buffer solution prepared using NaCl, HAc, NaAc, and $C_6H_5Na_3O_7{\cdot}2H_2O$ was used to stabilize the ionic strength of the solution to improve the accuracy of analysis. All the chemicals used were of analytical reagent grade.

2.2. Adsorbents preparation

The Ce-WTRS particles were prepared by impregnation method. Every 4 g of WTRS particles (−100 + 120 mesh size) were added into 100 mL cerium nitrate solution (0.006 mol/L) and the contents (WTRS particles/aqueous solution = 40 g/L) were kept for constant heating in digital thermostat water bath pot (HH-4, Shanghai Guohua, China) at 363 K for 2 h. These particles were heated in the muffle furnace (SXL-1008, Shanghai Jinghong, China) at 473 K for 4 h. The cerium-modified adsorbent (Ce-WTRS) was obtained and used in batch experiments.

2.3. Characterization of adsorbents

The major chemical elements of WTRS and Ce-WTRS were determined using energy dispersive X-ray spectrometer (EDX) (EDX-LE, Shimadzu, Japan). The surface area and pore size analyzer (F-Sorb 3400, Beijing App-one, China) helped to determine the structure of the adsorbents. The qualitative identification of chemical groups and compounds in WTRS and Ce-WTRS was identified by Fourier transform infrared spectrometer (FTIR) (IR Prestige-21, Shimadzu, Japan). X-ray diffraction analyzer (XRD) (D-8 Diffractometer, Brucker, Germany) was used to identify the crystal structure of the adsorbents. The morphology feature of the surface was examined with field-emission scanning electron microscope (SEM) (Hitachi S-4700, Shimadzu, Japan).

2.4. Analysis methods

The fluoride concentration was determined using fluoride ion selective electrode (pF-1, Shanghai Rex, China) with pH meter (pHS-3C, Shanghai Rex, China) according to ion selective electrode method. Different initial concentration of F^- solutions were prepared by proper dilution from F^- stock solution (1,000 mg/L). Necessary amount of adsorbent material was taken in a 250 mL polyethylene plastic bottle and 100 mL of fluoride solution of known concentration was added.

The mixtures were shaken on the water-bathing constant temperature vibrator (SHZ-82, Shanghai Guohua, China) for required time.

The extent of F^- adsorption (q_e), the percent removal of F^-, the amount desorbed of fluoride (q_d), and the desorption ratio of F^- were estimated using the following equations:

$$q_e = \frac{C_0 - C_e V_a}{W} \quad (1)$$

$$\text{Removal rate} = \frac{C_0 - C_e}{C_0} \times 100\% \quad (2)$$

$$q_d = \frac{C_{\text{sol}} V_d}{W} \quad (3)$$

$$\text{Desorption rate} = \frac{\text{released } F^- (\text{mg/g})}{\text{initially } F^- \text{adsorbed (mg/g)}} \times 100\% \quad (4)$$

All the investigations were carried out in duplicate and the average values were reported herein to confirm reproducibility of the experimental results.

2.5. Kinetics experiments

The kinetic studies were conducted by batch mode. Fixed dosage (1 g/100 mL) of adsorbent was added into a set of polyethylene plastic bottles containing 100 mL sodium fluoride with the concentration of 50 mg/L. The mixtures were agitated at 120 rpm and 303 K. The samples were taken out at preset time intervals to monitor the residual concentration of F^-. To increase the comparability, similar kinetic experiments of various F^- concentrations (100, 200 mg/L) were also carried out.

2.6. Effect of pH

(1) About 1 g of adsorbent materials and 100 mL fluoride solution were added into a set of polyethylene plastic bottles, respectively. About 50 and 100 mg/L were selected as the initial concentration, respectively. The mixtures were agitated at 120 rpm and 303 K. In certain time intervals, the samples were taken to test the pH.

(2) About 1 g of adsorbent materials and 100 mL fluoride solution were added into a set of polyethylene plastic bottles, respectively. The effect of pH on F^- adsorption was investigated by adjusting solution pH to 1, 3, 5, 7, 9, and 11 with the initial F^- concentration of 50 mg/L, respectively. The mixtures were agitated at 120 rpm and 303 K for 4 h. The equilibrium pH and F^- removal rate were examined.

2.7. Thermodynamic experiments

One gram of adsorbent materials and 100 mL fluoride solution of various initial concentrations (10, 20, 50, 100, 200, and 300 mg/L) were added into a set of polyethylene plastic bottles, respectively. The mixed suspensions were agitated at 120 rpm for 4 h. Fluoride adsorption experiments were carried out at 303, 318, 333, and 348 K, respectively. The pH of the F^- solution was kept primordially without any adjustment.

2.8. Desorption and readsorption experiments

Desorption experiment of F^- was performed as follows: 1 g of absorbent was used to adsorb 100 mL (V_a) F^- solution (50 mg/L) for 4 h. The adsorbed adsorbents were filtered and washed gently more than three times with deionized water to remove any residual F^- unabsorbed. The fluoride-loaded adsorbent was treated by 50 mL (V_d) of sodium hydroxide solution at different concentrations (0.001–0.050 mol/L) to desorb the fluoride. The mixtures were shaken for 4 h (a period equal to the adsorption time) and filtered for defluorination analysis. The above-mentioned defluorinated adsorbent, which had been treated by NaOH (0.01 mol/L) for 4 h, was again treated with 100 mL of fluoride solution at 50 mg/L for readsorption analysis.

3. Results and discussion

3.1. Characterization of adsorbents

The EDX patterns of WTRS and Ce-WTRS are shown in Fig. 1(a) and (c). Results indicated that the elements such as silicon, aluminum, iron, potassium, calcium, magnesium oxygen, and carbon were found on both adsorbents. Furthermore, cerium was found on the surface of Ce-WTRS. The results of EDX analysis are in accordance with the XRD patterns (Fig. 2). Characteristic peaks of SiO_2, Al_2O_3, and Fe_2O_3 were observed on the XRD diagrams of WTRS and Ce-WTRS. Peak at 28° corresponding to CeO_2, which may be formed by alteration of Ce^{3+} due to the heated treatment, indicated the existence of cerium in Ce-WTRS.

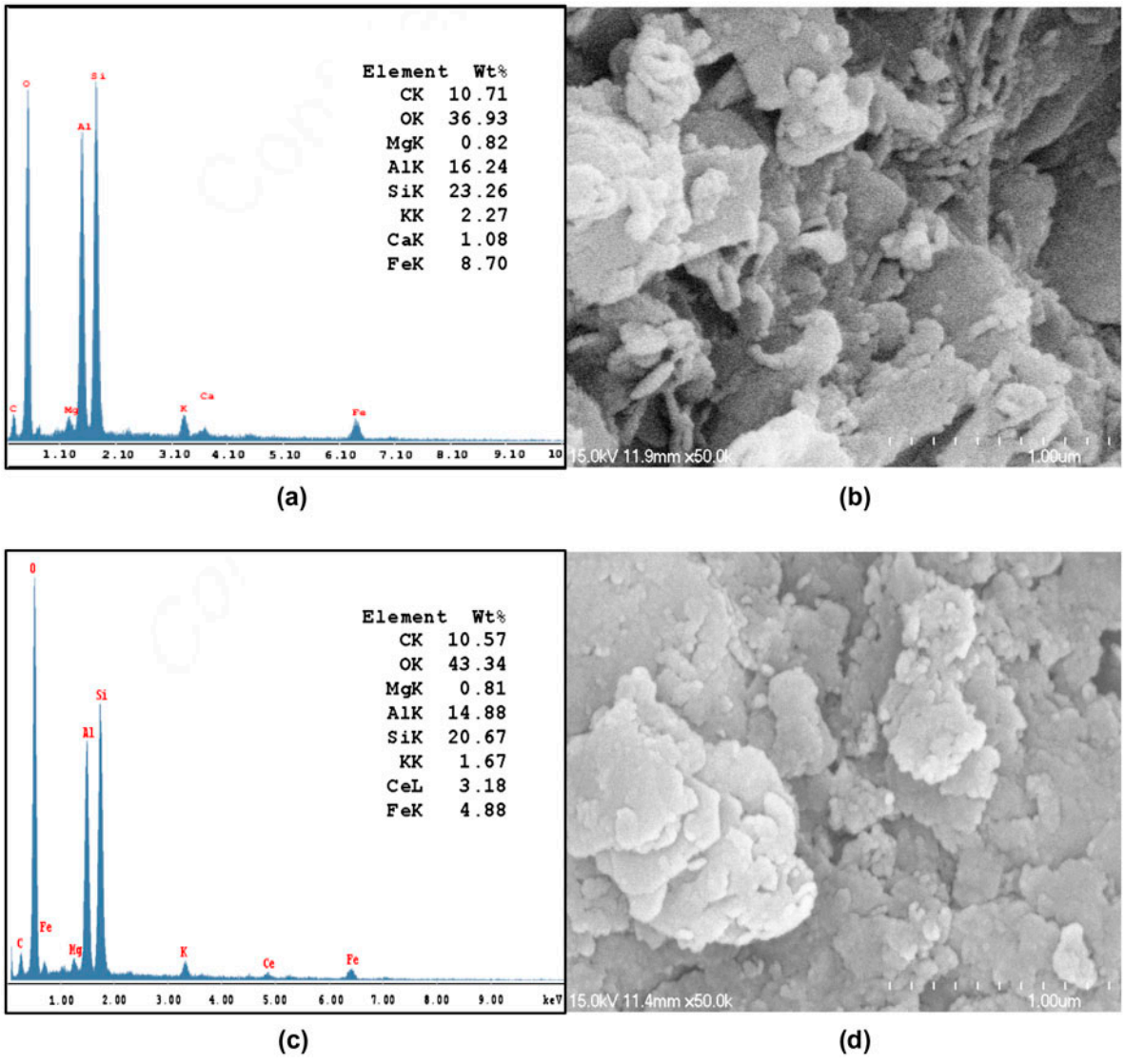

Fig. 1. EDX image of: (a) WTRS, (c) Ce-WTRS, and SEM image of: (b) WTRS, (d) Ce-WTRS.

SEM micrographs of WTRS (Fig. 1(b)) and Ce-WTRS (Fig. 1(d)) reveal that both adsorbents possess heterogeneous lamellar structure with tiny pore and holes. The surface area of Ce-WTRS and WTRS is found to be 50.26 and 54.38 m^2/g and the pore volume is 0.0175 and 0.0182 mL/g, respectively. No obvious difference was found between Ce-WTRS and WTRS. It was reasonable to believe that the structure of Ce-WTRS was similar to WTRS.

Fig. 3 represents the FTIR spectra of WTRS and Ce-WTRS before and after adsorption. The broad band in the range of 3,650–3,200/cm is due to the stretching mode of structural OH groups. The band at 1,640/cm generally corresponds to the OH bending mode of water. The metal–oxygen groups are observed at 470, 798, and 1,035/cm, corresponding to Al–O, Si–O–Si, and Al–OH stretching mode, respectively. After adsorption, the band observed at 3,440/cm becomes strong and sharp. It is inferred that OH groups and metal–oxygen groups have been taking part in the adsorption procedure.

3.2. Kinetic analysis

3.2.1. Effect of contact time

The effect of contract time on adsorption of F^- is presented in Fig. 4. The time of adsorption equilibrium is found to be 120 min for Ce-WTRS, which is earlier than WTRS (150 min). It is evidence that there

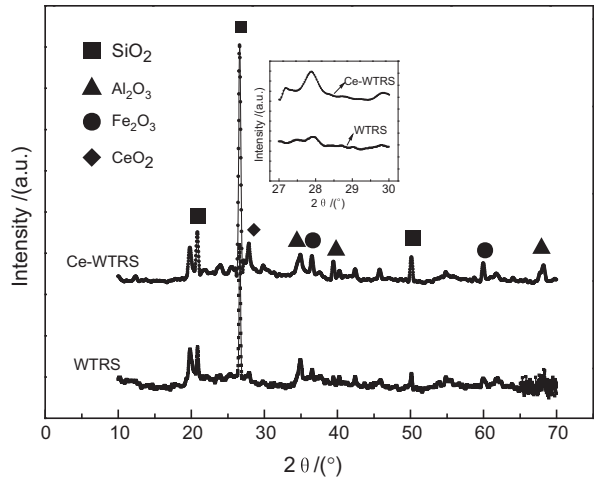

Fig. 2. XRD diagrams of WTRS and Ce-WTRS.

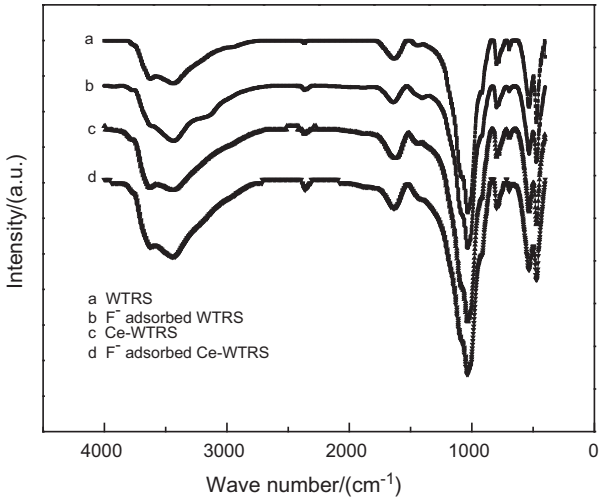

Fig. 3. FTIR spectra of (a) WTRS, (b) F^- adsorbed WTRS, (c) Ce-WTRS, and (d) F^- adsorbed Ce-WTRS.

are more active adsorption sites on the adsorbents after cerium modification. The optimal contract time is selected to be 240 min for sufficient adsorption.

3.2.2. Kinetic models

The experimental data were fitted to pseudo-first-order, pseudo-second-order, and intra-particle diffusion models to understand the adsorption type and mechanism.

The pseudo-first-order and pseudo-second-order kinetic models represent physisorption and chemisorption, respectively. The pseudo-first-order and pseudo-second-order equations are expressed as:

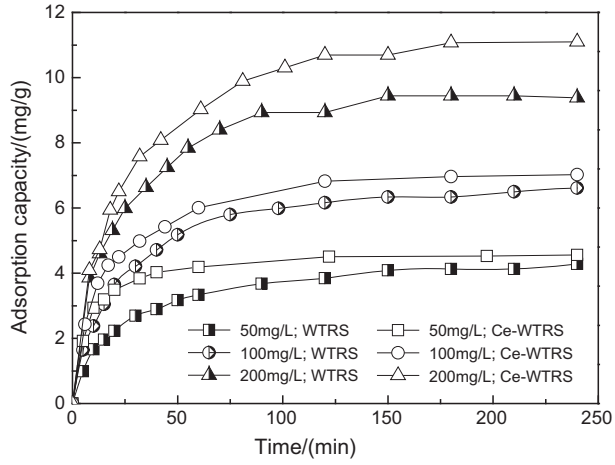

Fig. 4. Effect of contract time on F^- removal by WTRS and Ce-WTRS (initial concentration of F^- = 50–200 mg/L, adsorbent dosage = 10 g/L, temperature = 303 K, pH was not adjusted).

$$\ln(q_e - q_t) = \ln q_e - k_1 t \tag{5}$$

$$\frac{t}{q_t} = \frac{1}{k_2 q_e^2} + \frac{1}{q_e} t \tag{6}$$

The intra-particle diffusion model, which could determine the diffusion mechanism of F^- in adsorption process, is suggested as:

$$q_t = k_{id} t^{1/2} + C_i \tag{7}$$

3.2.3. Evaluation of kinetic models

3.2.3.1. Pseudo-first-order and pseudo-second-order kinetic models. Linear plots of t/q_t vs. t (Fig. 5(a1) and (a2)) and ln $(q_e - q_t)$ vs. t (Fig. 5(b1) and (b2)) were used to fit the pseudo-first-order and pseudo-second-order kinetic models, respectively. The rate constants (k_1, k_2) and equilibrium absorption capacity (q_e) are given in Table 1 along with the correlation coefficient (R^2). The values of correlation coefficients indicate that the pseudo-second-order model provides a better relationship for kinetics. In addition, the calculated equilibrium adsorption capacities ($q_{e,\mathrm{cal}}$) obtained from pseudo-second-order model are more close to the experimental values ($q_{e,\mathrm{exp}}$). Accordingly, the surface reaction involving complexation or ion exchange is the main mechanism of adsorption.

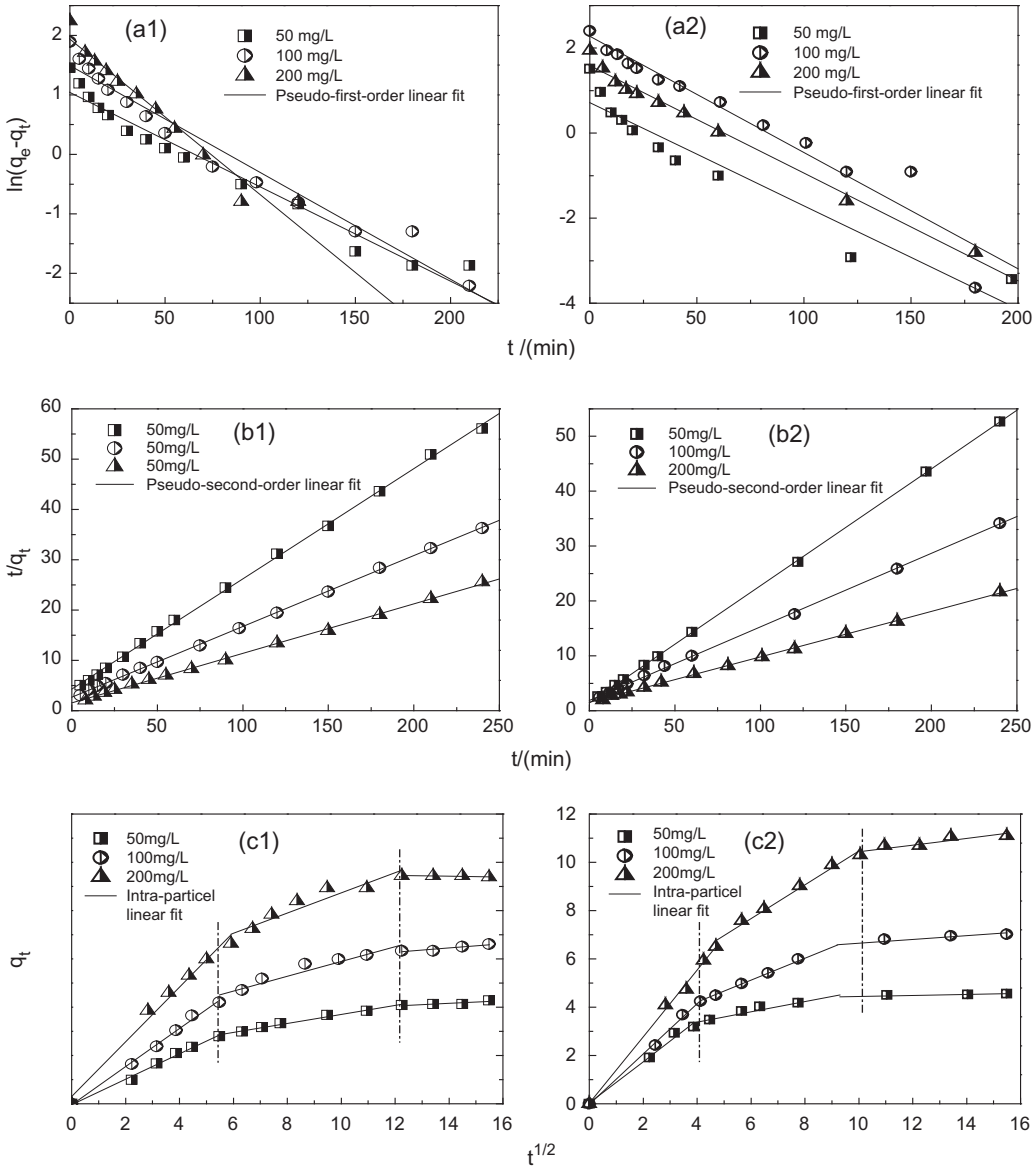

Fig. 5. Adsorption kinetic models for fluoride onto WTRS and Ce-WTRS (initial concentration of F^- = 50–200 mg/L, adsorbent dosage = 10 g/L, temperature = 303 K, pH was not adjusted).

3.2.3.2. Intra-particle diffusion model. The adsorption process of adsorbate ions from aqueous solution onto the adsorbent generally involves three stages [23]: (1) film diffusion; (2) intra-particle diffusion; (3) adsorption or ion exchange. In generally, the third step is assumed to be very fast and do not represent the rate-limiting step of the whole adsorption process [24]. So, the first two steps are always limiting the rate of adsorption.

To probe further into the rate of internal mass transfer, experimental data were fitted to the intra-particle diffusion model. If there is an excellent fit of the experimental data to the intra-particle diffusion model, the plot of q_t vs. $t^{1/2}$ should show a strong linear relationship. Further, the intra-particle diffusion is the only rate-determining step if the plots pass through the origin. However, it is clearly shown in Fig. 5(c1) and (c2) that the plots were not linear over the whole time range but multilinear. This indicates that both intra-particle diffusion and film diffusion contribute to the rate-determining step [25] of F^- adsorption.

Fig. 5(c1) and (c2) shows that all the plots can be divided into three sections. In the first section (from 0 to 20 min for Ce-WTRS and 0 to 30 min for WTRS,

Table 1
Adsorption kinetic constants of F^- onto WTRS and Ce-WTRS (temperature 303 K; adsorbent dosage 1 g/100 mL; agitation speed 120 rpm; pH was not adjusted)

	WTRS			Ce-WTRS		
C_0 (mg/L)	50	100	200	50	100	200
$q_{e,exp}$ (mg/g)	4.28	6.61	9.38	4.56	7.02	11.10
Pseudo-first-order kinetic model						
k_1	0.0159	0.0180	0.0261	0.0243	0.0253	0.0274
$q_{e,cal}$ (mg/g)	2.83	4.45	6.92	2.05	4.91	9.75
R^2	0.9626	0.9666	0.9573	0.9146	0.9883	0.9379
Pseudo-second-order kinetic model						
k_2 (g/mg min)	0.011	0.007	0.006	0.032	0.010	0.005
$q_{e,cal}$ (mg/g)	4.56	7.10	10.16	4.69	7.46	12.07
R^2	0.9992	0.9997	0.9990	0.9999	0.9995	0.9993

respectively), fluoride ions were transported to the outside surface of adsorbent via the boundary layer diffusion. At this stage, the adsorption of fluoride occurred through external surface adsorption until the surface adsorption sites were saturated. Thereafter, the fluoride ions diffused into the internal pores of the adsorbents for further adsorption (from 20 to 120 min for Ce-WTRS and 30 to 150 min for WTRS, respectively). In this section, the F^- density gradient decreased gradually, and the adsorption of F^- was controlled by both film diffusion and intra-particle diffusion. The last section (from second section to 240 min) was the equilibrium adsorption stage where film diffusion and intra-particle diffusion began to slow down because of the extremely low fluoride concentration [26]. This type of mult-linearity has also reported in other researchers [23,25,27].

3.3. Effect of pH

Fig. 6 shows the pH history of the solution during adsorption process. It can be seen from Fig. 6 that the pH decreases sharply when the adsorbents were added. It has been known that OH group is easy to take off the proton to reduce the pH. So, it is reasonable to say that the surface of Ce-WTRS is richer in OH groups as the decrease of pH for Ce-WTRS seems quite greater. It further indicates that the addition of Ce causes rise of the –OH activity. For WTRS (Fig. 6(a)), the curves show fast decrease firstly and slight decline subsequently. While for Ce-WTRS (Fig. 6(b)), the pH curves show rapid advances at the first 25 min and then decline with time. This could be related to the reactions occurred in the solid/liquid system. Hydrolysis reaction of fluoride ions would happen in aqueous:

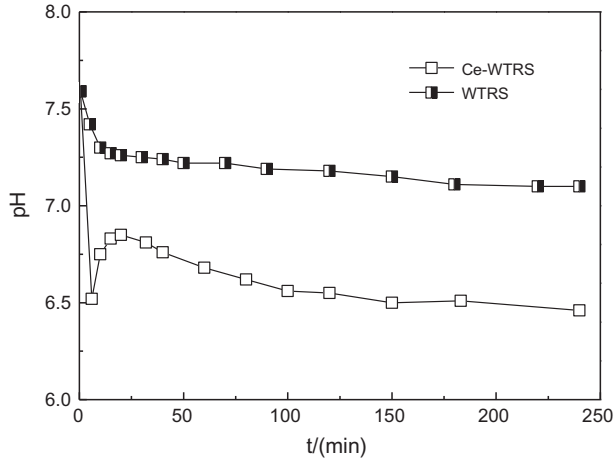

Fig. 6. pH history of the solution (initial F^- concentration = 50 mg/L, adsorbent dosage = 10 g/L, temperature = 303 K, pH was not adjusted).

$$F^- + H_2O \Leftrightarrow HF + OH^- \quad \Delta H_+ > 0, \Delta H_- < 0 \tag{8}$$

Complex reaction between F^- and the metal composition occurred via the general reaction formula:

$$R_xM_yO_z(OH)_t + nF^- \rightarrow [R_xM_yO_z(OH)_t]F^{n-} \quad (R, M = \text{Al, Fe, Ce, Si, } C, N, K \text{ and so on})\Delta H < 0 \tag{9}$$

And ion exchange between F^- and –OH happens as follows:

$$W - OH + F^- = W - F + OH^- \quad (W = \text{WTRS or Ce-WTRS})\Delta H > 0 \tag{10}$$

On the one hand, the decrease of F^- caused by the complex reaction (Eq. (9)) would give rise to the leftward move of the hydrolysis reaction (Eq. (8)), i.e. OH^- numbers in decline. So, the pH of the solution kept falling down. On the other hand, ion exchange between F^- and –OH (Eq. (10)) would make fun of pH. This suggests that the complex reaction (Eq. (9)) may be the primary reaction in the process of F^- adsorption onto WTRS. The double trends for Ce-WTRS indicate that the surface reaction (Eq. (9)) and ion exchange (Eq. (10)) should be simultaneous.

The effect of initial pH of solution on F^- adsorption is shown in Fig. 7. The equilibrium pH increased with the initial pH from 1 to 7, while declined with the initial pH from 7 to 11. In the case of pH around 1, the fluoride species existed mainly in the form of HF which were uncharged and were hardly attached on the adsorbents. While negatively charged F^- dominated at higher pH values. Hydroxyl in strong alkaline solution could well competitively adsorb on the active adsorption sites with fluoride, resulting in reduced adsorption efficiency. In the intermediate range, both species coexisted with one another [28]. Plateaus were found at pH 3–9 for both adsorbents and the maximum fluoride adsorption capacity was obtained at this range. It is proved that the adsorption of fluoride is pH dependent, and the optimum pH range for fluoride removal is between 3 and 9. The pH of the system was not adjusted because the initial and equilibrium pH of fluoride solution were right in this range.

3.4. Isotherms analysis

3.4.1. Effect of temperature and initial concentration

Fig. 8 illustrates the effect of temperature on F^- adsorption. The F^- uptake of Ce-WTRS was more substantial than WTRS. As the initial fluoride concentration of 300 mg/L, the adsorption capacity increased from 11.76 to 14.69 mg/g at 348 K. The enhanced adsorption capacity might be due to the availability of adsorption sites that increased with cerium treatment. The adsorption uptake increased as temperature rose, which indicates that the adsorption of fluoride onto adsorbent materials is favorable at high temperature.

As seen in Fig. 8, the adsorption capacity of fluoride increased with increasing the initial F^- concentration. This could be explained by the increasing driving force of F^- onto active sites in high concentration solution. The uptake of fluoride changed little as the initial concentration of F^- rose to a certain degree because of the saturation of adsorption site.

3.4.2. Adsorption isotherms

Equilibrium data, commonly known as adsorption isotherms, are basic requirement for the design of adsorption system [29]. The equilibrium data were tested with respect to Langmuir, Freundlich, Dubinin–Radushkevich, and Temkin isotherm models in order to obtain the best-fit.

The Langmuir equation is valid for monolayer sorption which is known as the ideal localized monolayer model [30] and given as:

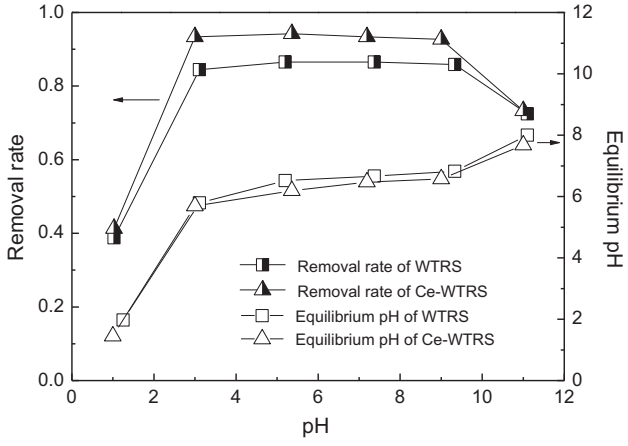

Fig. 7. Effect of pH on F^- removal by WTRS and Ce-WTRS (initial concentration of F^- = 50 mg/L, adsorbent dosage = 10 g/L, temperature = 303 K, initial pH 1–11).

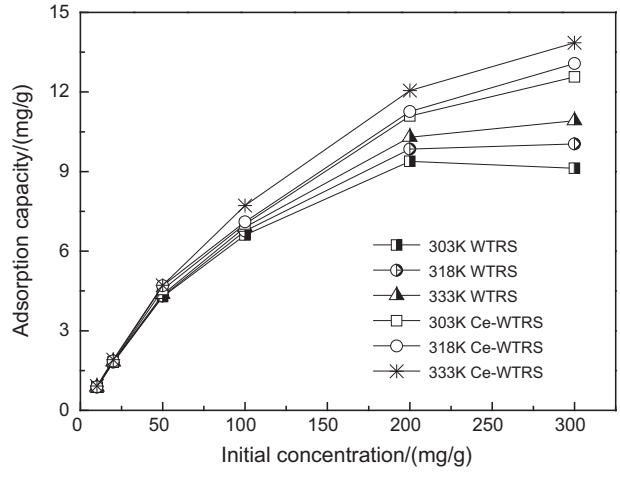

Fig. 8. Effects of temperature and initial concentration on fluoride removal by WTRS and Ce-WTRS (initial concentration of F^- = 10–300 mg/L, adsorbent dosage = 10 g/L, temperature = 303 K, pH was not adjusted).

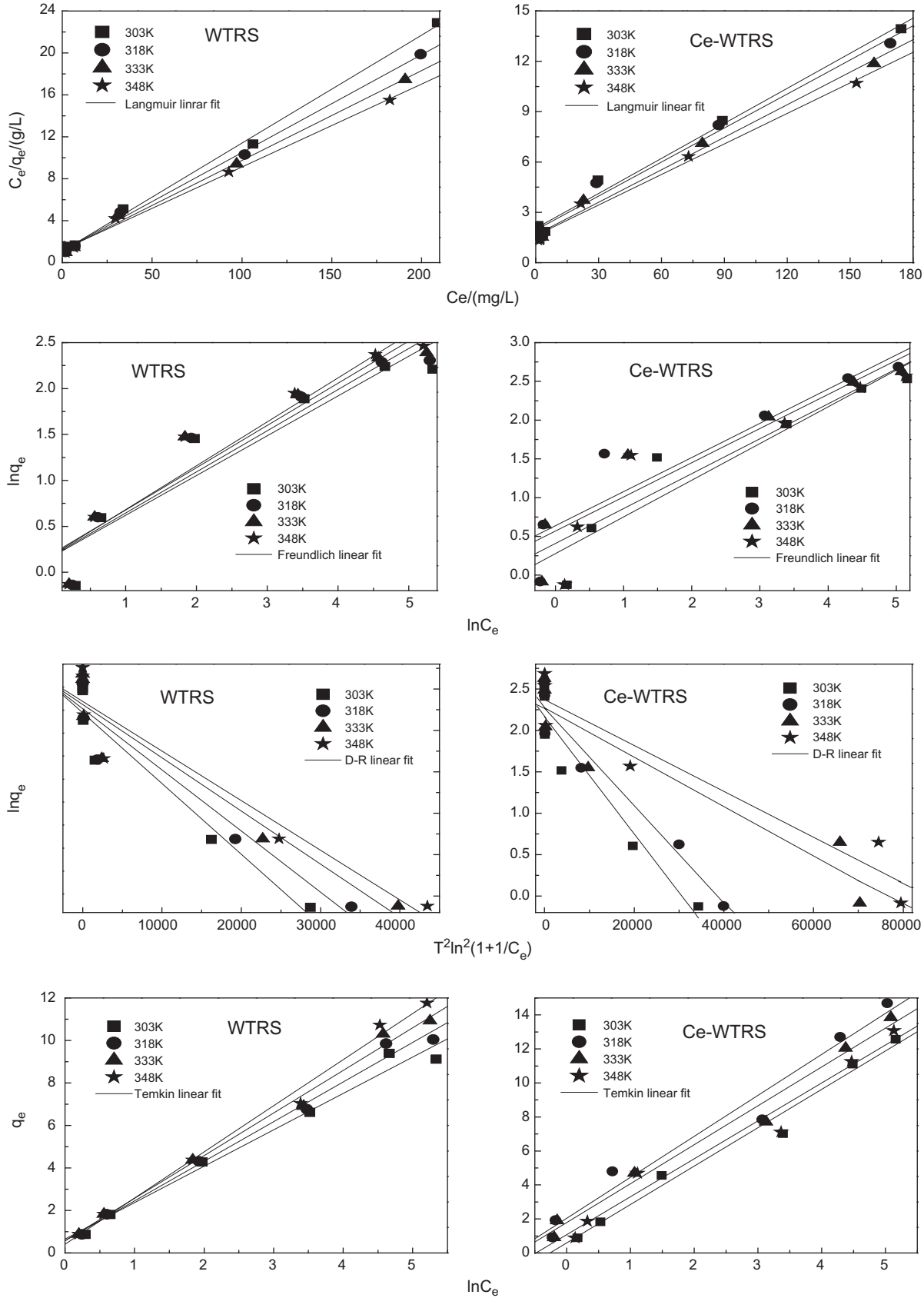

Fig. 9. Adsorption isotherm models for fluoride onto WTRS and Ce-WTRS (initial concentration of F^- = 10–300 mg/L, adsorbent dosage = 10 g/L, temperature = 303 K, pH was not adjusted).

Table 2
Isotherm constants for F^- adsorption onto WTRS and Ce-WTRS at different temperatures (initial F^- concentration 10–300 mg/L; adsorbent dosage 1 g/100 mL; contract time 4 h; pH was not adjusted)

	WTRS				Ce-WTRS			
	303 K	318 K	333 K	348 K	303 K	318 K	333 K	348 K
Langmuir								
q_m	9.71	10.71	11.66	12.64	13.47	13.87	14.52	15.45
K_L	0.094	0.080	0.073	0.065	0.063	0.067	0.088	0.089
R^2	0.9971	0.9976	0.9969	0.9959	0.9905	0.9860	0.9917	0.9894
R_L	0.034–0.517	0.041–0.554	0.044–0.578	0.049–0.606	0.050–0.614	0.047–0.599	0.037–0.532	0.036–0.530
Freundlich								
K_F	1.208	1.220	1.248	1.229	1.320	1.505	1.767	1.890
n	2.313	2.236	2.180	2.096	2.112	2.219	2.272	2.268
R^2	0.8902	0.9043	0.9109	0.9209	0.8979	0.8603	0.8878	0.8660
Dubinin–Radushkevich								
q_m	7.18	7.50	7.85	8.12	8.69	9.65	9.71	10.70
R^2	0.9311	0.9214	0.9158	0.9066	0.9226	0.9504	0.8970	0.9204
Temkin								
B	1.71	1.86	2.01	2.17	2.26	2.23	2.29	2.41
R^2	0.9824	0.9903	0.9924	0.9922	0.9815	0.9668	0.9830	0.9726

Table 3
Comparisons of fluoride adsorption capacity of WTRS and Ce-WTRS with other adsorbents

Adsorbent	pH	Concentration range (mg/L)	Temperature (K)	q_m (mg/g)	Reference
Fe–Al–Ce trimetal oxide adsorbent	7.0	85.4	298	178.00	[18]
Activated alumina	7.0	2.5–14.0	–	2.41	[31]
Magnesium-doped nanoranged hematite	7.0	10–150	308	75.2	[32]
Pine bark biochar	2.0	1–100	308	10.53	[33]
Meixnerite	–	12.4–248	293±2	19.10	[34]
Fe–Al mixed hydroxide	4.0	10–90	303	91.70	[35]
CeO_2/Al_2O_3 composites	3–10	20–200	303	37.00	[36]
Alum sludge	6.0	5.0–35.0	305	5.39	[37]
Algal biosorbent	7.0	5.0–25.0	303	1.27	[38]
Alumina supported carbon nanotube	3.0	–	298	45.32	[39]
Apatitic tricalcium phosphate	6.8–6.9	30–60	313	15.42	[40]
Ca/650	6.9 ± 0.1	210.0	298	19.05	[41]
Magnetic-chitosan particles	7.0 ± 0.2	5–140	291–293	22.49	[42]
Metal ion loaded natural zeolite	–	1–20	303	2.04–4.13	[43]
WTRS	Without adjustment	10–300	348	12.64	Present study
Ce-WTRS	Without adjustment	10–300	348	15.45	Present study

$$\frac{C_e}{q_e} = \frac{1}{K_L q_m} + \frac{C_e}{q_m} \quad (11)$$

$$R_L = \frac{1}{1 + K_L C_0} \quad (12)$$

Dimensionless parameter of the equilibrium or adsorption intensity R_L, which is often used for further analysis of adsorption, is calculated as:

The isotherm shape can be indicated as below according to the values of R_L: $R_L > 1$ for unfavorable adsorption; $R_L = 1$ for linear adsorption; $0 < R_L < 1$ for

favorable adsorption; and $R_L = 0$ for irreversible adsorption.

Freundlich isotherm model is described as a non-ideal adsorption which is based on multilayer adsorption and commonly presented as:

$$\ln q_e = \ln K_F + \frac{1}{n}\ln C_e \tag{13}$$

The Dubinin–Radushkevich (D–R) isotherm model agrees with the assumption that the adsorbate is adsorbed through porous structure. The D–R equation is represented as:

$$\ln q_e = \ln q_m - \beta\varepsilon^2 \text{ where } \varepsilon = RT\ln\left(1+\frac{1}{C_e}\right) \text{ and } E = -\frac{1}{\sqrt{2\beta}} \text{ or } \frac{1}{\sqrt{-2\beta}} \tag{14}$$

The Temkin isotherm is an adsorption model based on the heat of ion exchange between adsorbate and adsorbent. The Temkin equation is given as:

$$q_e = B\ln K_T + B\ln C_e \text{ where } \frac{RT}{b} = B \tag{15}$$

3.4.3. Evaluation of adsorption isotherms

The adsorption isotherm plots of Langmuir, Freundlich, D–R model, and Temkin model are presented in Fig. 9. The isotherm parameters (q_m, K_L, R_L, K_F, n, B) along with the correlation coefficients (R^2) are summarized in Table 2. The values of R^2 indicate that the fitting order of the isotherm models is: Langmuir > Temkin > D–R > Freundlich. The best fit of Langmuir model infers that fluoride adsorption onto adsorbent materials is monolayer chemisorption. The Langmuir constant K_L for Ce-WTRS increased with increasing temperature, indicating that the adsorption process is endothermic. And the process of fluoride onto WTRS is proved to be exothermic as the values of K_L decreased as the temperature rose. The values of R_L at all temperatures are between 0 and 1, demonstrating that the adsorption of F^- is favorable at experimental conditions. The experimental data can also fit the Temkin model well. It is indicated that the fluoride removal by the materials is mainly governed by ion exchange. The Temkin constant B increased with the temperature rose, suggesting an enhanced adsorption activity at high temperature. The poorly fit of Freundlich and D–R isotherms confirms that fluoride adsorption onto adsorbents is not multilayer and the structure of adsorbents is not multihole.

The maximum adsorption capacity (q_m) obtained from Langmuir isotherm model is usually used for the comparison of different sorbents. The different values of q_m depend on the diverse characteristics of the adsorbents, various surface modification methods, and varying experimental conditions. The maximum fluoride adsorption capacity (q_m) of Ce-WTRS obtained at 348 K was 15.45 mg/g, 22% higher than WTRS (12.64 mg/g). We can see in Table 3 that the fluoride removal by WTRS and Ce-WTRS is considerably effective, compared with other adsorbents.

3.4.4. Thermodynamics for adsorption

Thermodynamics parameters can provide valuable knowledge to clarify the adsorption mechanism. The Gibbs free energy change (ΔG^θ) is determined using K_L values obtained from the Langmuir model by the formula:

$$\Delta G^\theta = -RT\ln K_L \tag{16}$$

The standard enthalpy change (ΔH^θ) and standard entropy change (ΔS^θ) are given by Van't Hoff equation as follows:

$$\ln K_L = \frac{\Delta S^\theta}{R} - \frac{\Delta H^\theta}{RT} \tag{17}$$

ΔH^θ and ΔS^θ were calculated from the intercept and slope of the plot of ln K_L vs. $1/T$ (Fig. 10). The values of thermodynamic parameters (ΔG^θ, ΔH^θ and ΔS^θ) are listed in Table 4.

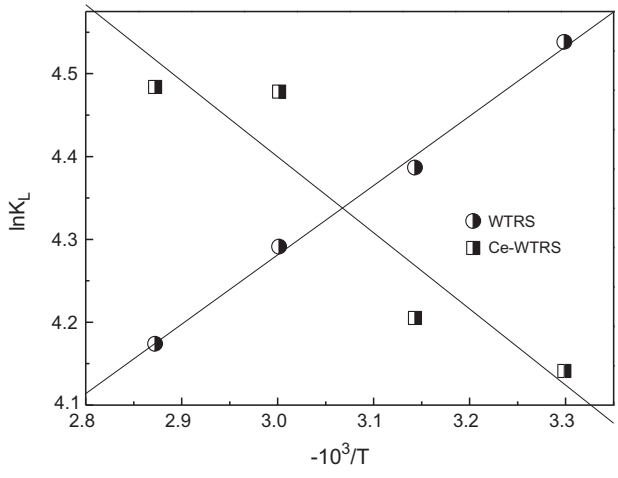

Fig. 10. Van't Hoff plots for the adsorption of fluoride onto WTRS and Ce-WTRS.

Table 4
Thermodynamic parameters for the adsorption of fluoride onto WTRS and Ce-WTRS

	WTRS			Ce-WTRS		
Temperature (K)	ΔG^{θ} (kJ/mol)	ΔH^{θ} (kJ/mol)	ΔS^{θ} (J/mol K)	ΔG^{θ} (kJ/mol)	ΔH^{θ} (kJ/mol)	ΔS^{θ} (J/mol K)
303	−11.439	−6.965	14.701	−10.437	7.636	59.488
318	−11.604			−11.124		
333	−11.886			−12.405		
348	−12.082			−12.980		

Table 5
Data for F^- desorption using different concentrations of NaOH (%)

		Rate of desorption at different concentration of NaOH							
Absorbent	Rate of adsorption	0.001 mol/L	0.002 mol/L	0.005 mol/L	0.007 mol/L	0.010 mol/L	0.020 mol/L	0.050 mol/L	Rate of readsorption
WTRS	77	7	10	19	24	25	16	2	27
Ce-WTRS	78	11	15	33	38	41	23	2	36

The negative values of ΔG^{θ} suggest that the adsorption process is feasible and spontaneous. Positive values of ΔS^{θ} can be interrelated to the increased randomness at the solid–liquid interface during the adsorption process. Positive value of ΔH^{θ} for F^- onto Ce-WTRS suggests the endothermic nature. Accordingly, the ion exchange of F^- and $-OH$ was involved in fluoride adsorption because energy was needed for hydroxyls to leave the surface and for F^- to combining with the active adsorption sites. While negative value of ΔH^{θ} of F^- removal by WTRS indicates an exothermic process. So, the key reaction of F^- onto WTRS is considered to be the complexation reaction (Eq. (9)). In general, isometric heat for chemical adsorption, which is similar to chemical reaction heat, is above 40 kJ/mol. The absolute values of ΔH^{θ} that were all below this value might be explained by the fact that chemical reactions between F^- and metal ions as well as ion exchange between F^- and –OH occurred simultaneously.

3.5. Desorption and readsorption studies

It is expected that OH^- can compete greatly with F^- adsorbed already. Hence, NaOH solution was used to desorb fluoride from the adsorbents. The effect of initial concentration of NaOH on desorption is shown in Table 5. The best desorption efficiency of F^- was reached to 41% for Ce-WTRS when the NaOH concentration was 0.01 mol/L. Desorption of fluoride ions occurring in alkaline solution confirms that the ion exchange between F^- and –OH is involved in F^- adsorption. The incomplete desorption of F^- shows that ion exchange mechanism is not unique. Other mechanism, such as surface complexation reaction (Eq. (9)) is also considered to explain the F^- adsorption process. Further study of the regenerated adsorbent for reutilization was conducted. The fluoride-loaded adsorbents treated with 0.01 mol/L of NaOH for 12 h were used. The readsorption percentage of fluoride onto Ce-WTRS was found to be 36%. The regeneration and readsorption capacities of WTRS were also investigated and their values were 25 and 27%, respectively. The poor desorption rate and regeneration rate indicate that the regeneration and reuse of adsorbent are impracticable, but it provides a basis for understanding the mechanism of F^- adsorption onto adsorbents.

4. Conclusions

WTRS particles were used as fluoride adsorbents for resource utilization. Results showed that the chemical composition and structure of Ce-WTRS were similar to WTRS. The pseudo-second-order kinetic model was the best-fit for fluoride removal, suggesting that chemisorption was the main adsorption mechanism.

Further analyses by intra-particle diffusion model indicated that the rate-controlling steps were dominated by both film diffusion and intra-particle diffusion. The optimal range of pH for F^- adsorption was 3–9. Ce-WTRS were found to be more efficient for fluoride removal compared to WTRS. The maximum fluoride adsorption capacity (q_m) of Ce-WTRS determined by Langmuir isotherm model was 15.45 mg/g, a considerable value compared with other fluoride adsorbents. The Langmuir and Temkin adsorption isotherm models were considered as the best-fit. It confirmed that the adsorption process of F^- was monolayer chemisorption. The negative values of ΔG^θ indicated that the adsorption of F^- was feasible and spontaneous. $\Delta H^\theta > 0$ for Ce-WTRS indicated an endothermic adsorption process and $\Delta H^\theta < 0$ for WTRS demonstrated an exothermic nature. Surface complexation and ion exchange were seen as the mechanism of F^- onto WTRS and Ce-WTRS.

Acknowledgment

The authors gratefully acknowledge the National Natural Science Foundation of China (No. 50878136) and the project of Suzhou Science and Technology Bureau (No. SYG201122) for the financial supports.

Nomenclatures

b	—	Temkin isotherm constant (kJ/mol)
B	—	constant of Temkin isotherm
C_0	—	initial concentration of fluoride in solution (mg/L)
C_e	—	concentration of fluoride in solution at equilibrium (mg/L)
C_i	—	intra-particle diffusion model constant
C_{sol}	—	concentration of the solution after desorption (mg/L)
E	—	adsorption freedom energy (kJ/mol)
k_1	—	pseudo-first-order rate constant of adsorption (1/min)
k_2	—	pseudo-second-order rate constant of adsorption [(g/mg) min]
K_{id}	—	intra-particle rate constant (mg/g/min$^{1/2}$)
K_F	—	Freundlich constant [(mg/g) (L/g)$^{1/n}$]
K_L	—	Langmuir constant (L/mg)
K_T	—	Temkin constant (L/mg)
$1/n$	—	Freundlich exponent
q_d	—	desorption capacity of the adsorbent (mg/g)
q_e	—	adsorption capacity of the adsorbent at equilibrium (mg/g)
$q_{e,cal}$	—	the calculated equilibrium adsorption capacity (mg/g)
$q_{e,exp}$	—	the experimental equilibrium adsorption capacity (mg/g)
q_m	—	maximum adsorption capacity (mg/g)
q_t	—	adsorption capacity at time t (min)
R	—	ideal gas constant (8.314 J/mol K)
R^2	—	correlation coefficient
R_L	—	adsorption intensity
T	—	time (min)
T	—	temperature (K)
V_a	—	solution volume for adsorption (mL)
V_d	—	solution volume for desorption (mL)
W	—	amount of adsorbent added (g)
G^θ	—	Gibbs free energy (kJ/mol)
H^θ	—	enthalpy of adsorption (kJ/mol)
S^θ	—	entropy of adsorption (kJ/mol K)
B	—	Dubinin–Radushkevich model constant
E	—	Polanyi potential (J/mol)

References

[1] M.K. Gibbons, D.U.D.o. Civil, R.E.C.E. Program, The Use of Water Treatment Residual Solids for Arsenate and Phosphate Adsorption, Dalhousie University, Halifax, 2009.
[2] E.A. Dayton, N.T. Basta, C.A. Jakober, J.A. Hattey, Using treatment residuals to reduce phosphorus in agricultural runoff, J. Am. Water Works Ass. 95 (2003) 151–158.
[3] C.-H. Wang, S.-J. Gao, T.-X. Wang, B.-H. Tian, Y.-S. Pei, Effectiveness of sequential thermal and acid activation on phosphorus removal by ferric and alum water treatment residuals, Chem. Eng. J. 172 (2011) 885–891.
[4] Y. Yang, Y.Q. Zhao, A.O. Babatunde, L. Wang, Y.X. Ren, Y. Han, Characteristics and mechanisms of phosphate adsorption on dewatered alum sludge, Sep. Purif. Technol. 51 (2006) 193–200.
[5] K.C. Makris, D. Sarkar, R. Datta, Aluminum-based drinking-water treatment residuals: A novel sorbent for perchlorate removal, Environ. Pollut. 140 (2006) 9–12.
[6] A. Hovsepyan, J.-C.J. Bonzongo, Aluminum drinking water treatment residuals (Al-WTRs) as sorbent for mercury: Implications for soil remediation, J. Hazard. Mater. 164 (2009) 73–80.
[7] Y.-S. Kim, D.-H. Kim, J.-S. Yang, K. Baek, Adsorption characteristics of As(III) and As(V) on alum sludge from water purification facilities, Sep. Purif. Technol. 47 (2012) 2211–2217.
[8] E.J. Reardon, Y. Wang, A limestone reactor for fluoride removal from wastewaters, Environ. Sci. Technol. 34 (2000) 3247–3253.
[9] A.H. Essadki, B. Gourich, C. Vial, H. Delmas, M. Bennajah, Defluoridation of drinking water by electrocoagulation/electroflotation in a stirred tank reactor with a comparative performance to an external-loop airlift reactor, J. Hazard. Mater. 168 (2009) 1325–1333.
[10] A.H. Essadki, B. Gourich, M. Azzi, C. Vial, H. Delmas, Kinetic study of defluoridation of drinking water by electrocoagulation/electroflotation in a stirred tank reactor and in an external-loop airlift reactor, Chem. Eng. J. 164 (2010) 106–114.
[11] S. Lahnid, M. Tahaikt, K. Elaroui, I. Idrissi, M. Hafsi, I. Laaziz, Z. Amor, F. Tiyal, A. Elmidaoui, Economic evaluation of fluoride removal by electrodialysis, Desalination 230 (2008) 213–219.

[12] S.K. Nath, R.K. Dutta, Acid-enhanced limestone defluoridation in column reactor using oxalic acid, Process Saf. Environ. Prot. 90 (2012) 65–75.
[13] H. Cui, Q. Li, Y. Qian, R. Tang, H. An, J. Zhai, Defluoridation of water via electrically controlled anion exchange by polyaniline modified electrode reactor, Water Res. 45 (2011) 5736–5744.
[14] B.R. Min, A.L. Gill, W.N. Gill, A note on fluoride removal by reverse osmosis, Desalination 49 (1984) 89–93.
[15] N. Viswanathan, S. Meenakshi, Selective fluoride adsorption by a hydrotalcite/chitosan composite, Appl. Clay Sci. 48 (2010) 607–611.
[16] S.K. Swain, T. Patnaik, R.K. Dey, Efficient removal of fluoride using new composite material of biopolymer alginate entrapped mixed metal oxide nanomaterials, Desalin. Water Treat. 51 (2013) 4368–4378.
[17] S. Kagne, S. Jagtap, D. Thakare, S. Devotta, S.S. Rayalu, Bleaching powder: A versatile adsorbent for the removal of fluoride from aqueous solution, Desalination 243 (2009) 22–31.
[18] X. Wu, Y. Zhang, X. Dou, M. Yang, Fluoride removal performance of a novel Fe–Al–Ce trimetal oxide adsorbent, Chemosphere 69 (2007) 1758–1764.
[19] T. Zhang, Q. Li, Y. Liu, Y. Duan, W. Zhang, Equilibrium and kinetics studies of fluoride ions adsorption on CeO_2/Al_2O_3 composites pretreated with non-thermal plasma, Chem. Eng. J. 168 (2011) 665–671.
[20] S.K. Swain, S. Mishra, T. Patnaik, R.K. Patel, U. Jha, R.K. Dey, Fluoride removal performance of a new hybrid sorbent of Zr(IV)–ethylenediamine, Chem. Eng. J. 184 (2012) 72–81.
[21] M.S. Onyango, Y. Kojima, O. Aoyi, E.C. Bernardo, H. Matsuda, Adsorption equilibrium modeling and solution chemistry dependence of fluoride removal from water by trivalent-cation-exchanged zeolite F-9, J. Colloid Interface Sci. 279 (2004) 341–350.
[22] S.K. Swain, T. Padhi, T. Patnaik, R.K. Patel, U. Jha, R.K. Dey, Kinetics and thermodynamics of fluoride removal using cerium-impregnated chitosan, Desalin. Water Treat. 13 (2010) 369–381.
[23] L. Ding, H. Deng, C. Wu, X. Han, Affecting factors, equilibrium, kinetics and thermodynamics of bromide removal from aqueous solutions by MIEX resin, Chem. Eng. J. 181–182 (2012) 360–370.
[24] C. Sun, G. Zhang, R. Qu, Y. Yu, Removal of transition metal ions from aqueous solution by crosslinked polystyrene-supported bis-8-oxyquinoline-terminated open-chain crown ethers, Chem. Eng. J. 170 (2011) 250–257.
[25] A.K. Bhattacharya, T.K. Naiya, S.N. Mandal, S.K. Das, Adsorption, kinetics and equilibrium studies on removal of Cr(VI) from aqueous solutions using different low-cost adsorbents, Chem. Eng. J. 137 (2008) 529–541.
[26] K.S. Tong, M.J. Kassim, A. Azraa, Adsorption of copper ion from its aqueous solution by a novel biosorbent Uncaria gambir: Equilibrium, kinetics, and thermodynamic studies, Chem. Eng. J. 170 (2011) 145–153.
[27] A.O. Babatunde, Y.Q. Zhao, Equilibrium and kinetic analysis of phosphorus adsorption from aqueous solution using waste alum sludge, J. Hazard. Mater. 184 (2010) 746–752.
[28] Y. Kim, C. Kim, I. Choi, S. Rengaraj, J. Yi, Arsenic removal using mesoporous alumina prepared via a templating method, Environ. Sci. Technol. 38 (2003) 924–931.
[29] K. Kadirvelu, C. Karthika, N. Vennilamani, S. Pattabhi, Activated carbon from industrial solid waste as an adsorbent for the removal of Rhodamine-B from aqueous solution: Kinetic and equilibrium studies, Chemosphere 60 (2005) 1009–1017.
[30] S. Guo, W. Li, L. Zhang, J. Peng, H. Xia, S. Zhang, Kinetics and equilibrium adsorption study of lead(II) onto the low cost adsorbent—Eupatorium adenophorum spreng, Process Saf. Environ. Prot. 87 (2009) 343–351.
[31] S. Ghorai, K.K. Pant, Equilibrium, kinetics and breakthrough studies for adsorption of fluoride on activated alumina, Sep. Purif. Technol. 42 (2005) 265–271.
[32] M. Mohapatra, T. Padhi, S. Anand, B.K. Mishra, CTAB mediated Mg-doped nano Fe_2O_3: Synthesis, characterization, and fluoride adsorption behavior, Desalin. Water Treat. 50 (2012) 376–386.
[33] D. Mohan, R. Sharma, V.K. Singh, P. Steele, C.U. Pittman, Fluoride removal from water using bio-char, a green waste, low-cost adsorbent: Equilibrium uptake and sorption dynamics modeling, Ind. Eng. Chem. Res. 51 (2011) 900–914.
[34] Q. Guo, E.J. Reardon, Fluoride removal from water by meixnerite and its calcination product, Appl. Clay Sci. 56 (2012) 7–15.
[35] M.G. Sujana, G. Soma, N. Vasumathi, S. Anand, Studies on fluoride adsorption capacities of amorphous Fe/Al mixed hydroxides from aqueous solutions, J. Fluorine Chem. 130 (2009) 749–754.
[36] T. Zhang, Q. Li, Z. Mei, H. Xiao, H. Lu, Y. Zhou, Adsorption of fluoride ions onto non-thermal plasma-modified CeO_2/Al_2O_3 composites, Desalin. Water Treat. (2013) 1–10. doi:10.1080/19443994.2013.800324.
[37] M.G. Sujana, R.S. Thakur, S.B. Rao, Removal of fluoride from aqueous solution by using alum sludge, J. Colloid Interface Sci. 206 (1998) 94–101.
[38] S. Venkata Mohan, S.V. Ramanaiah, B. Rajkumar, P.N. Sarma, Removal of fluoride from aqueous phase by biosorption onto algal biosorbent Spirogyra sp.-IO2: Sorption mechanism elucidation, J. Hazard. Mater. 141 (2007) 465–474.
[39] Y.H. Li, S. Wang, X. Zhang, J. Wei, C. Xu, Z. Luan, D. Wu, B. Wei, Removal of fluoride from water by carbon nanotube supported alumina, Environ. Technol. 24 (2003) 391–398.
[40] M. Mourabet, A. El Rhilassi, M. Bennani-Ziatni, R. El Hamri, A. Taitai, Studies on fluoride adsorption by apatitic tricalcium phosphate (ATCP) from aqueous solution, Desalin. Water Treat. 51 (2013) 6743–6754.

[41] E. Tchomgui-Kamga, E. Ngameni, A. Darchen, Evaluation of removal efficiency of fluoride from aqueous solution using new charcoals that contain calcium compounds, J. Colloid Interface Sci. 346 (2010) 494–499.
[42] W. Ma, F.-Q. Ya, M. Han, R. Wang, Characteristics of equilibrium, kinetics studies for adsorption of fluoride on magnetic-chitosan particle, J. Hazard. Mater. 143 (2007) 296–302.
[43] S. Samatya, Ü. Yüksel, M. Yüksel, N. Kabay, Removal of fluoride from water by metal ions (Al^{3+}, La^{3+} and ZrO^{2+}) loaded natural zeolite, Sep. Purif. Technol. 42 (2007) 2033–2047.